agronomy

MDPI

Article

Modeling the Droplet Size Distribution of Atomizers with Different Cage Diameters for Large-Payload Unmanned Aerial Vehicles (UAVs)

Jiajun Yang [1,2], Longlong Li [2], Qing Tang [2], Peng Hu [2], Wenlong Yan [2] and Ruirui Zhang [1,*]

[1] School of Mechanical and Electrical Engineering, Xinjiang Agricultural University, Urumqi 830052, China; 17311715713@163.com
[2] Research Center for Intelligent Equipment, Beijing Academy of Agriculture and Forestry Sciences, Beijing 100097, China; lill@nercita.org.cn (L.L.); tangq@nercita.org.cn (Q.T.); hp2469730431@163.com (P.H.); 2222216001@stmail.ujs.edu.cn (W.Y.)
* Correspondence: zhangrr@nercita.org.cn; Tel.: +86-010-51503991

Abstract: Spraying drift is a key concern in aerial spraying and relates closely to droplet size. With the growing application of large-load UAVs, large-load plant protection UAVs lack corresponding spraying devices. The rotary cage atomizer, suitable for high-flow aerial spraying, is a better option for large-load plant protection UAVs' spraying needs. A modified rotating cage atomizer based on the AU5000 atomizer in manned aircraft was designed, with cage diameters of 76 mm, 86 mm, 96 mm, 106 mm, and 116 mm. Based on the IEA-I high-speed wind tunnel, this study investigated the impacts of different wind speeds, flow rates, and cage diameters on the atomization characteristic distribution of the modified atomizer and established a model. The results show that when other variables remain constant, for every 1 mm increase in cage diameter, the average droplet size decreases by 0.944 μm. The R^2 of the predicted values and the measured values of the droplet size model is 0.917. Under the conditions of 50 m/s, 58.3 m/s, and 66.6 m/s wind speeds, as the cage diameter increases, Relative Span (RS) shows a trend of first increasing and then decreasing. Among them, the RS of the 106 mm cage diameter is usually the highest. This study can provide a reference for the aerial spraying scheme of large-payload plant protection UAVs, such as the selection of the diameter of the rotating cage.

Keywords: droplet size; atomization characteristics; rotary cage atomizer; aerial application; high-speed wind tunnel

check for updates

Academic Editor: Andrea Peruzzi

Received: 24 January 2025
Revised: 1 March 2025
Accepted: 2 March 2025
Published: 4 March 2025

Citation: Yang, J.; Li, L.; Tang, Q.; Hu, P.; Yan, W.; Zhang, R. Modeling the Droplet Size Distribution of Atomizers with Different Cage Diameters for Large-Payload Unmanned Aerial Vehicles (UAVs). *Agronomy* **2025**, *15*, 647. https://doi.org/10.3390/agronomy15030647

Copyright: © 2025 by the authors. Licensee MDPI, Basel, Switzerland. This article is an open access article distributed under the terms and conditions of the Creative Commons Attribution (CC BY) license (https://creativecommons.org/licenses/by/4.0/).

1. Introduction

Plant protection UAVs, which have strong terrain adaptability and high operational efficiency, are widely used in spraying operations [1,2]. However, the payload capacity of plant protection UAVs is a key factor that limits their operational efficiency [3]. To break through this limitation, in recent years, relevant research on large-payload plant protection UAVs has been carried out successively in the world. Compared with light-duty plant protection UAVs, large-payload UAVs have a faster flight speed and a wider spraying width. Therefore, the required flow rate will also increase [4]. The commonly used nozzles for light-duty plant protection UAVs are pressure nozzles and rotary disk atomizers. If pressure nozzles are used for operation, in order to meet the flow rate requirements, a large number of nozzles will be added to the spray boom [5]. This will increase the load on the aircraft and make the installation process more cumbersome, and the reduction in the distance between the nozzles will also lead to mutual interference between the sprays,

resulting in poor spraying effects. If rotary disk atomizers are used, an increase in the flow rate will cause the resistance of the rotary disk motor to increase exponentially, leading to an increase in power consumption [6]. Therefore, it is necessary to develop spraying devices suitable for large-payload UAVs.

In agricultural aerial spraying operations, the size of the droplets is one of the key factors affecting droplet drift [7]. Specifically, large-sized droplets have a fast sedimentation rate and a relatively strong drifting ability. However, when they collide with leaves, they are prone to bouncing and breaking, which causes pesticide loss. Small-sized droplets have a slower deposition rate and are more affected by the lateral wind field, thus being more likely to drift [8]. Spray drift can cause pesticides to deviate from the target area, which will result in ineffective losses of pesticides, impact the effectiveness of pest and disease control, and simultaneously bring about serious environmental pollution problems [9]. Precisely controlling the droplet size during the application process of plant protection machinery and obtaining a narrower droplet spectrum are of crucial importance for achieving efficient pest and disease control and reducing pesticide pollution [10]. In centrifugal atomization technology, which is currently recognized as an advanced technology that produces droplets with good uniformity and a narrower droplet spectrum, the mainstream products are divided into two categories: rotary disk atomizers and rotary-cage atomizers [11]. Among them, the rotating cage atomizer has the advantages of high operation speed, high efficiency [12], large spraying flow rate, and controllable droplet size, and it is very suitable as a nozzle in the field of aerial pesticide application by large-payload UAVs. However, there is still some room for optimization. Specifically, the rotating-cage atomizer mainly achieves the control of the droplet size by adjusting the rotational speed. As a key component of the atomizer for breaking up droplets, the rotating cage also has a significant impact on aspects such as the atomization effect and droplet distribution. Therefore, by optimizing the structural parameters of the rotating cage, the overall performance of the atomizer can be improved.

To date, extensive research has been conducted on rotary cage atomizers. For instance, Elsaied et al. developed a three-dimensional computational fluid dynamics (CFD) model to evaluate the concept of a rotating cage sprayer setup in orchard spraying, aiming to reduce drift without decreasing biological efficiency [13]; Teske et al. compared the droplet size distribution of AU5000 and AU4000 in a wind tunnel by changing wind speed, fan blade angle, and flow conditions [14]; Hewitt et al. measured the spray droplet spectra of different rotary cage atomizers when they were operating under specific pressures [15]; Matsushita conducted spray flow analysis on high-speed rotary cage atomizers by using the LES (Large Eddy Simulation) and k-ε two-equation model [16]. Maximilian et al. analyzed the droplet size and spray velocity generated by a rotating cage atomizer using phase-Doppler measurement technology [17]. The above studies have concentrated on research on the original cage diameter (86 mm) of the atomizer. When conducting large-scale plant protection operations, the range of droplet sizes generated by an atomizer with a single cage diameter is limited, and the relationship between multiple cage diameters and droplet sizes remains unclear.

In this study, taking the structure of the AU5000 atomizer as a reference, a modified rotary cage atomizer with different cage diameter specifications was designed. By using the IEA-I high-speed wind tunnel [18] and the Malvern Spraytec spray particle size analyzer [19], the atomization characteristics of the atomizer under different conditions of cage diameters, flow rates, and wind speeds were measured, and the influence of different cage diameters on the atomization effect of the atomizer was analyzed. Furthermore, with the rotational speed as an intermediate variable, a model including the diameter, rotational speed, flow rate, wind speed, and droplet size was established, and the stability of the

model was verified. This study aims to provide a theoretical reference for the design and application of atomizers so as to effectively reduce droplet drift and improve the utilization rate of pesticides.

2. Materials and Methods

2.1. Rotating Cage Design of Atomizer

In this study, a modified atomizer was designed based on the structure of the AU5000 atomizer (produced by Micronair) [20]. The modified atomizer is capable of bearing a flow rate that spans 0~23 L·min^{-1}, and it weighs 1.8 kg in total. The atomizer consists of six mechanisms: an installation clamp, inlet valve, adjustable fan blades (adjustment range 25~85°) [21], rotating cage bottom, rotating cage, and internal network pipe. The rotary cage connects the entire atomizer through screws, with threaded holes provided at its rear part for connection to the bottom plate of the rotary cage, and the rotary cage bottom can ensure that the rotary cage does not deform during high-speed rotation. The rotary cage, installed outside and rotating coaxially with the internal network pipe, enables the liquid to undergo secondary atomization, while the internal network pipe is for primary atomization [22]. The inlet valve is used to connect external pipelines and allow liquid to enter the atomizer. The atomizer can adjust the rotation speed by changing the angle of the fan blades. The rotation speed ranges from 0 to 10,000 r·min^{-1}. The installation clamp serves to firmly fix the atomizer onto the spray boom or rack. Figure 1 presents a photograph and a structural schematic of the atomizer.

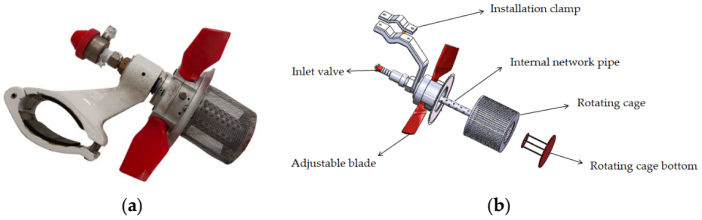


Figure 1. Modified atomizer. (**a**) Photograph of atomizer; (**b**) schematic diagram of atomizer structure.

In order to analyze the influence of cage diameter on atomization characteristics and establish a model, this study was based on the original cage diameter of the AU5000 atomizer. Four other cages with different diameters at a gradient of 10 mm were designed. The other structural parameters of the designed rotary cages with different diameters should be kept consistent with those of the original rotary cage, namely, the inner diameter is 60 mm, the mesh size of the cage is 1 mm, and the height of the cage is 76 mm. A schematic diagram of the parameters of rotating cages with different diameters is shown in Figure 2.

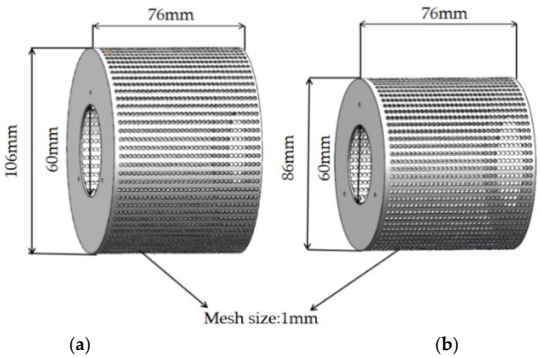


Figure 2. Schematic diagram of parameters of rotating cages with different diameters; (**a**) 106 mm; (**b**) 86 mm.

2.2. Experimental Platforms

In order to study the influence of different wind speeds, flow rates, and cage diameters on the atomization characteristics of the atomizer and establish a droplet size model, a wind tunnel test platform that can precisely control the wind speed, flow rate and atomizer rotation speed was built based on the IEA-I high-speed wind tunnel self-constructed by the Beijing Academy of Agriculture and Forestry Sciences, as shown in Figure 3.



Figure 3. Wind tunnel measurement platform. (**a**) Schematic diagram of wind tunnel measurement platform; (**b**) location of atomizer, wind tunnel, and spray particle size analyzer; (**c**) rotational atomization of atomizer and spray detection; (**d**) photograph of the high-speed wind tunnel.

The platform includes an IEA-I high-speed wind tunnel, wind tunnel control platform, tanks, liquid supply device, lifting platform, flow detection device, spray detection device, computer, and new-type atomizer. The liquid supply device selects the Prodn750 W water pump produced by Prodn Intelligent Control Electronic Technology Co., Ltd., Wuhu, China. Its maximum flow rate is 33.3 L·min^{-1}, the pressure adjustment range is 0~0.4 MPa, and the

precision is 0.01 Pa. The flow detection device selects the HSTL-N type flowmeter produced by Suwei Technology Co., Ltd., Guangzhou, China. Its maximum range is 20 L·min^{-1}, and the maximum error is 0.5% [23]. The rotational speed measuring device uses the Sw6234c non-contact tachometer (produced by Beijing Huakong Xingye Technology Development Co., Ltd. Beijing, China). Its maximum measurable rotational speed is 99,999 r·min^{-1}, and the maximum error is 0.1 r·min^{-1} [24]. The droplet detection device selects the Spraytec spray particle size analyzer produced by Malvern Panalytical Ltd., Malvern, UK.

This particle size analyzer uses a 300 μm lens, and the detection range of droplet size is 0.1~900 μm, with a maximum error of 0.01 μm [19]. The parameters of the spray particle size analyzer are shown in Table 1.

Table 1. Parameters of Spraytec spray particle size analyzer.

Parameter	Value
Lens focal length (μm)	300
Measurement range (μm)	0.1~900
Maximum error (μm)	0.01
Minimum scattering quantity	250
Minimum signal transmission capacity	10%

To minimize instrument errors, a pre-measurement calibration was performed. The steps included the following: aiming a tachometer at the stationary atomizer for a 0 r·min^{-1} reading, correcting any zero-point drift per the manual while ensuring the reflective strip was clear; using the spray particle size analyzer's built-in tool to focus the laser and detector, cleaning lenses before each test and taking multiple readings for accuracy; connecting the calibrated flowmeter to a standard one, measuring multiple flow points, computing errors, and applying the stable-flow accuracy to eliminate errors in the range; following the flowmeter calibration protocol, connecting the pump, flowmeter, and standard flowmeter in series, setting the pump to 50% output, and running it three times at that level for precision.

The wind tunnel adopts a direct-current open self-priming design, with a maximum power of 75 KW [18]. The wind speed (y) and wind tunnel motor frequency (x) have a favorable linear correlation, for which the correlation curve is fitted as $y = 0.58x + 0.13$ and the coefficient of determination R^2 is 0.967. This enables the simulation of the operating conditions of flying agricultural large-payload UAVs and the performance of related spray tests [25]. The parameters of the IEA-I high-speed wind tunnel are shown in Table 2.

Table 2. Parameters of the IEA-I high-speed wind tunnel.

Parameter	Value
Overall dimension (m)	9.8 × 1.2 × 1.8
Wind speed (m·s^{-1})	6.7–98
Turbulence intensity	<1.0%
Outlet diameter of contraction section (mm)	300
Averaged flow inclination angle	<0.2°

The atomizer is fixed at a position 0.2 m away from the center of the wind tunnel outlet, and the distance between the atomizer and the front end of the spray particle size analyzer is 0.5 m. The temperature is controlled between 20 °C and 22 °C, and the humidity is maintained between 50% and 70% [26].

2.3. Experimental Program

With the development of smart agriculture and artificial intelligence, in addition to directly developing large-payload UAVs, the transformation of manned aircraft to unmanned aircraft is also an important development trend for large-payload UAVs [27]. In this study, based on the application flow rate and operating speed of manned aircraft [28], combined with the working parameters of wind tunnel and atomizer experimental equipment, four kinds of wind speeds and five kinds of flow rates were comprehensively considered and set. The experimental projects and parameters are shown in Table 3.

Table 3. Experimental parameters.

Parameter	Value
Wind speed ($m \cdot s^{-1}$)	41.6, 50, 58.3, 66.6
Flow rate ($L \cdot min^{-1}$)	8.9, 10.6, 12.3, 13.9, 15.6
Cage diameter (mm)	76, 86, 96, 106, 116

The experiment adopted a three-factor full factorial design, with wind speed, cage diameter, and flow rate as independent variables. Specifically, each level of every factor was systematically combined with each level of the other factors to conduct experimental tests. There were 4 levels of wind speed, 5 levels of flow rate, and 5 levels of cage diameter. A total of 100 groups of experiments under different condition combinations were carried out.

During the experiment, the wind tunnel, water pump, flowmeter, and spray particle size analyzer were turned on in sequence, and the instruments were adjusted to the corresponding experimental parameters. After the wind speed had stabilized, the inlet valve of the atomizer was opened. When the spray became stable, the vertical height of the spray particle sizer was adjusted in steps of 0.1 mm via the lifting platform. When the laser beam had completely passed through the middle area of the spray, the detection button on the particle sizer was clicked to start the detection. Meanwhile, the tachometer was used to record the rotational speed of the atomizer and record the value shown on the flowmeter. Each group of experiments was repeated three times. After completing one group of experiments, parameter iteration was carried out (for example, replacing the rotating cage with a different diameter or adjusting the wind speed of the wind tunnel). The average value of each group of data was taken as the final data.

2.4. Data Processing

In this study, two parameters, Dv0.5 and RS, are adopted as the main parameters for evaluating the atomization effect of the atomizer. Dv0.5, measured in micrometers, represents the droplet diameter at which the cumulative distribution of droplets reaches 50%. That is, the volume of droplets with a diameter smaller than this value accounts for 50% of the total volume of all droplets. This is also known as the median volume diameter of droplets and serves as an indicator for measuring the droplet size [29]. The calculation formula for Dv0.5 is shown in Equation (1):

$$\mathrm{Dv0.5} = \left(\frac{\int_{Dmin}^{Dmax} D^3 dN}{\int_{Dmin}^{Dmax} D dN} \right)^{\frac{1}{3}} \quad (1)$$

In the formula, (D) represents the diameter of a droplet at any position within the atomization field, measured in meters; (N) represents the quantity of droplets whose diameter is (D).

The relative span of droplet size distribution (Relative Span, RS for short) serves as a significant index for evaluating the width of droplet size distribution in spraying. It characterizes the degree of dispersion of droplet sizes within the spray. Generally, the larger the RS value is, the lower the uniformity of droplets will be [30]. The calculation formula of RS is shown in Equation (2):

$$RS = \frac{Dv0.9 - Dv0.1}{Dv0.5} \quad (2)$$

In the formula, Dv0.1 represents the droplet diameter at which the cumulative volume distribution of droplets reaches 10%, measured in micrometers. That is to say, the volume of droplets with a diameter smaller than Dv0.1 accounts for 10% of the total volume of all droplets. Dv0.9 represents the droplet diameter at which the cumulative volume distribution of droplets reaches 90%, also measured in micrometers, meaning that the volume of droplets with a diameter smaller than Dv0.9 accounts for 90% of the total volume of all droplets.

2.5. Statistical Analysis

In this study, we used Stata 18.5 MP software for statistical analysis. Correlation analysis and the regression method were used to analyze the influences of wind speed, flow rate, and cage diameter on rotational speed, and a regression model was established. Correlation analysis and the regression method were also used to analyze the influences of wind speed, cage diameter, rotational speed, and flow rate on droplet size. Ridge regression was used to solve the multicollinearity problem existing in the droplet size model. The Bootstrap method was used to compare with the regression analysis to evaluate the stability of the model.

One-way ANOVA was used to analyze the influence of cage diameter on RS at each wind speed level. The confidence intervals for both models were calculated using the percentile method. For all statistical tests, unless otherwise specified, the statistical significance level was set at $p < 0.05$.

3. Results and Discussion

3.1. Analysis and Modeling of the Influence of Wind Speed, Flow Rate, and Cage Diameter on Rotational Speed

Rotation speed is a key factor in determining droplet size. Therefore, it was used as an intermediate variable in this study. To ensure accuracy, the atomizer fan angle was set at 55° [31].

The tachometer measurement results for rotational speed are presented in Figure 4. The rotational speed varies in the range of 1944~4983 r·min^{-1}. At the same flow rate and cage diameter, the rotational speed increases with the increase in wind speed; for example, under the conditions of a cage diameter of 86 mm and a flow rate of 8.9 L·min^{-1}, when the wind speed increases from 41.6 to 50 m/s, the rotational speed increases from 2329 to 3316 r·min^{-1}, with an increase of 42.3%. When the wind speed increases from 50 to 58.3 m/s, the rotational speed increases from 3316 to 3972 r·min^{-1}, with an increase of 19.7%. This indicates that as the wind speed continues to increase, the increase in rotational speed tends to be flattened. Under the same wind speed and flow rate, the rotational speed decreases as the cage diameter increases; however, there are exceptions, as shown in Figure 4d. Under the conditions of wind speed of 66.6 m/s and flow rate of 10.6 L·min^{-1}, when the cage diameter increases from 106 mm to 116 mm, the rotational speed increases from 4386 to 4409 r·min^{-1}. Similarly, under the same wind speed and cage diameter, as the flow rate increases, the rotational speed gradually shows a decreasing trend.

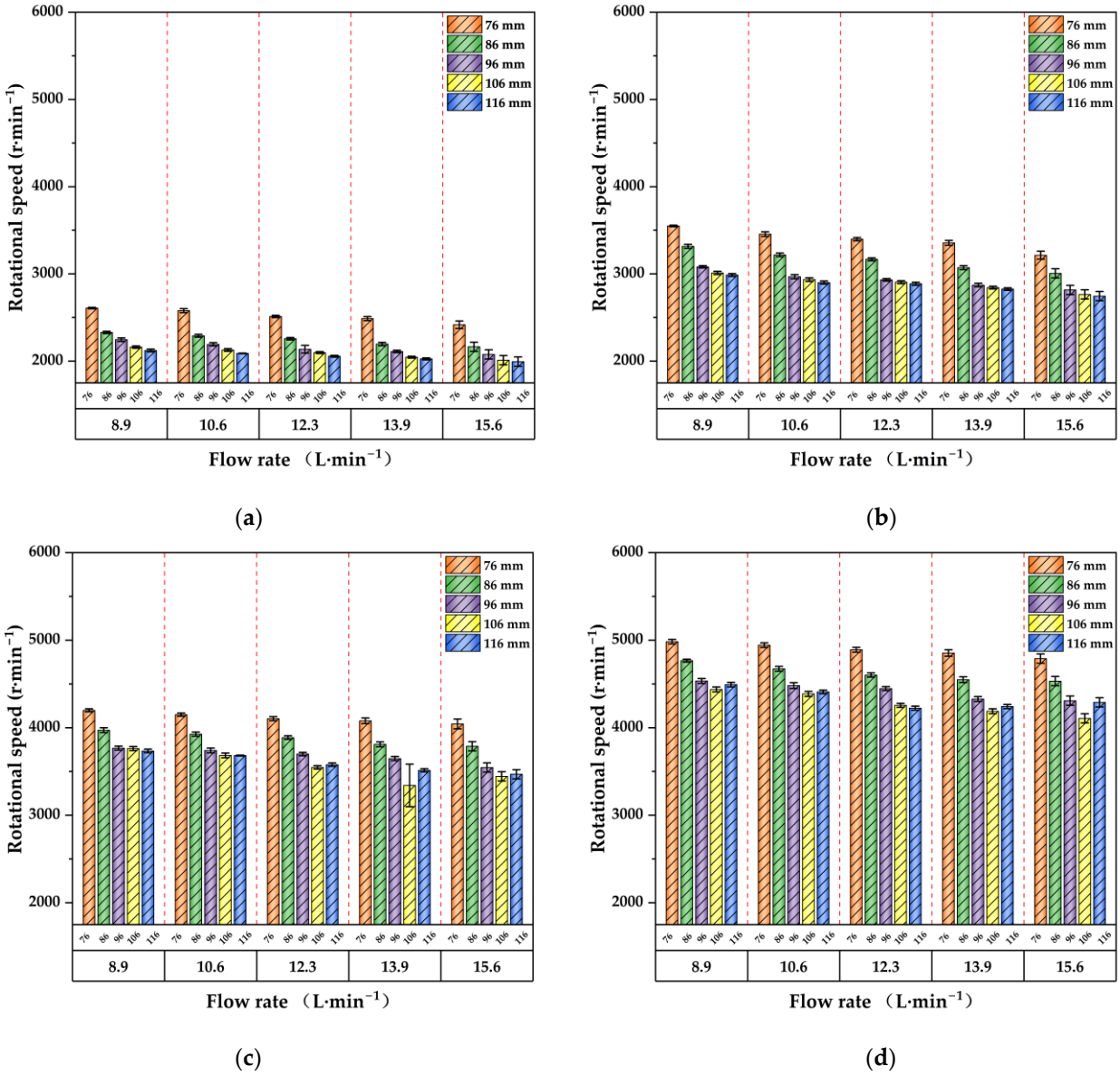


Figure 4. Relationship between cage diameter and rotational speed under different flow rates and wind speeds; (**a**) 41.6 m/s; (**b**) 50 m/s; (**c**) 58.3 m/s; (**d**) 66.6 m/s.

Correlation analyses evaluated the effects of wind speed, cage diameter, and flow rate on rotational speed (Table 4). Wind speed showed a strong positive correlation with rotational speed (r = 0.968, p = 0.001). Cage diameter had a significant negative correlation (r = −0.210, p = 0.036), while flow rate had no significant impact (r = −0.910, p = 0.367). Comprehensive analysis shows that among the parameters, wind speed has the greatest impact on rotational speed, while flow rate has the least.

Table 4. Correlation analysis of wind speed, diameter, and flow rate on rotational speed.

Parameter	Wind Speed ($m \cdot s^{-1}$)	Flow Rate ($L \cdot min^{-1}$)	Diameter (mm)
Significance value	0.001	0.367	0.036
Correlation coefficient	0.968	−0.910	−0.210

A significance test was performed on the regression coefficients. The linear regression model is as follows:

$$R = 110.79 + 91.29 \cdot W - 13.03D - 33.911 \cdot Q \quad (3)$$

The parameters in the model equation are represented by the following symbols: wind speed = W, rotational speed = R, flow rate = Q, cage diameter = D. The results of regression analysis are as follows: The coefficient of determination R^2 of the coefficient of determination model is 0.99, indicating that the variations in wind speed, cage diameter, and flow rate collectively explain 99% of the variation in rotational speed. According to the results of regression analysis, the *p*-value of the F test is 0.0001 (less than 0.05), indicating that the model is significant within the 95% confidence interval. Collinearity diagnosis was implemented. The results of the collinearity diagnosis show that the VIF values of all independent variables are 1.00, indicating that there is no multicollinearity problem in the model. The Durbin–Watson statistic is DW = 1.32, it is impossible to determine whether there is autocorrelation in the model residuals. Therefore, the Ljung–Box test was further carried out. The results show that, in the case of a lag of 10 orders, the *p*-value of the Ljung–Box test is 0.75, which is greater than the significance level of 0.05. It is considered that there is no significant autocorrelation in the model residuals. To evaluate the robustness of the model coefficient estimation, this study compared the results of the Bootstrap method with those of linear regression. The results showed that the results of the Bootstrap method were consistent with those of linear regression, indicating that the model established in this study has a certain degree of robustness.

Considering the possible overfitting risk, this study adopted two methods, namely, the comparison between predicted values and measured values and 10-fold cross-validation, to evaluate and judge whether overfitting occurred. Specifically, 50 sets of rotational speed data were used to compare and analyze the predicted values and measured values of rotational speed (Figure 5). The results indicated that the slope of the fitted straight line between the predicted and actual values was close to 1, with an R^2 of 0.959 for the fitted curve, and the maximum deviation between the predicted and actual values was 4.2%, with no outliers, suggesting a good fitting effect. The 10-fold cross-validation results showed that the average mean squared error (MSE) of the rotational speed prediction model was 8335.07. Together, the 50-group data validation (R^2 = 0.959) and 10-fold cross-validation (average MSE of 8335.07) demonstrated that the rotational speed prediction model had good generalization ability and no serious overfitting phenomenon.

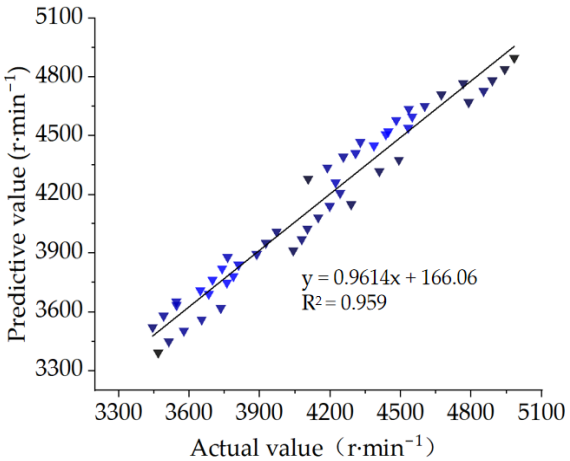


Figure 5. The predicted values and the actual values of the linear regression model for rotational speed.

3.2. Analysis and Modeling of the Effects of Wind Speed, Diameter, Flow Rate, and Rotational Speed on Droplet Size

3.2.1. Analysis of the Effects and Patterns of Different Parameters on Droplet Size

During aerial plant protection operations, due to the influence of multiple factors (such as atomizer parameters and environmental factors), droplets of different sizes will be generated. If the droplet size is too large or too small, it will affect the control effect of pests and diseases [32]. However, since environmental factors are difficult to control, accurately grasping the structural and operating parameters of the atomizer, deeply exploring the laws of the influence of different variables on droplet size, and constructing a precise model are of great significance for reducing spray drift and preventing pests and diseases. Table 5 shows the actual droplet size values for different parameters, ranging from 80 to 269 μm.

Table 5. Droplet size under different parameters.

Flow Rate ($L \cdot min^{-1}$)	Diameter (mm)	41.6 ($m \cdot s^{-1}$)	50 ($m \cdot s^{-1}$)	58.3 ($m \cdot s^{-1}$)	66.6 ($m \cdot s^{-1}$)
		Droplet Size at Four Different Wind Speeds (μm)			
8.9	76	248.0 ± 5.2	176.0 ± 4.0	128.5 ± 5.1	96.5 ± 3.4
	86	239.0 ± 5.1	168.0 ± 5.5	121.3 ± 4.0	91.3 ± 2.8
	96	236.0 ± 5.0	169.3 ± 3.8	116.0 ± 5.0	88.9 ± 3.8
	106	228.0 ± 2.0	151.1 ± 3.1	109.8 ± 5.0	81.5 ± 4.4
	116	225.0 ± 1.0	148.0 ± 3.0	107.6 ± 1.3	80.0 ± 2.7
10.6	76	253.0 ± 12.0	178.0 ± 8.0	130.0 ± 5.0	97.5 ± 2.0
	86	246.0 ± 11.8	172.4 ± 7.6	124.0 ± 4.9	92.7 ± 12.0
	96	242.0 ± 8.0	172.0 ± 5.0	119.5 ± 11.5	91.3 ± 7.5
	106	230.0 ± 4.6	157.9 ± 12.5	113.0 ± 8.2	83.2 ± 4.8
	116	227.0 ± 12.2	155.6 ± 7.3	112.3 ± 5.1	82.1 ± 4.0
12.3	76	258.2 ± 5.5	181.0 ± 8.0	131.6 ± 5.0	99.1 ± 1.7
	86	246.0 ± 12.0	173.1 ± 8.0	127.0 ± 2.6	93.3 ± 5.0
	96	243.0 ± 4.9	175.2 ± 7.8	121.3 ± 4.8	91.1 ± 5.0
	106	233.0 ± 12.0	162.1 ± 8.0	116 ± 5.0	84.5 ± 3.0
	116	230.0 ± 12.0	157.9 ± 8.2	114.7 ± 5.3	83.7 ± 4.0
13.9	76	266.0 ± 2.0	183.0 ± 2.0	133.4 ± 7.3	100.1 ± 4.6
	86	260.0 ± 0.6	182.0 ± 3.7	129.5 ± 3.7	98.2 ± 3.2
	96	248.0 ± 11.0	177.6 ± 9.3	126.7 ± 14.4	93.5 ± 11.6
	106	242.0 ± 7.3	165.3 ± 6.6	117.4 ± 19.5	88.6 ± 12.5
	116	238.0 ± 1.6	164.0 ± 8.0	116.5 ± 1.7	86.1 ± 3.1
15.6	76	269.0 ± 7.0	187.0 ± 5.0	135.6 ± 1.6	101.8 ± 4.5
	86	263.0 ± 4.6	184.0 ± 3.0	131.0 ± 11.0	99.1 ± 11.9
	96	258.0 ± 9.6	179.3 ± 2.1	127.7 ± 2.7	94.7 ± 7.0
	106	247.0 ± 7.0	168.2 ± 9.2	119.1 ± 7.0	89.2 ± 3.7
	116	241.0 ± 0.7	167.1 ± 1.3	117.3 ± 8.0	88.1 ± 1.3

Under the same flow rate and wind speed, as the cage diameter increases, the droplet size shows a gradually decreasing trend. The droplet size is the largest when the cage diameter is 76 mm and the smallest when the cage diameter is 116 mm (Table 5). The main reasons for this are as follows: when the cage diameter increases, the centrifugal force increases. As a result, the centrifugal force exerted on the liquid by the impact of the rotating cage increases, making it easier for the liquid to break up, thus leading to a reduction in the droplet size. According to the droplet breakup theory [33], during the process of liquid breakup, there is a force that resists the liquid's breakup. Assume this force is Fr. The force that prompts the droplets to break up is provided by the rotating cage,

and this force is equal to the centrifugal force Fc acting on the rotating cage. When Fc is much greater than Fr, the liquid is atomized.

Figure 6 is a schematic diagram showing the influence of different cage diameters on droplet size. As shown in Figure 6a, the larger cage diameter (d_1) corresponds to a relatively large centrifugal force (Fc_1). The degree of liquid fragmentation is relatively high, the liquid splits into more parts, and the droplet size is relatively small. As shown in Figure 6b, the smaller cage diameter (d_2) corresponds to a relatively small centrifugal force (Fc_2). The degree of liquid fragmentation is relatively low, the liquid splits less, and the droplet size is relatively large.

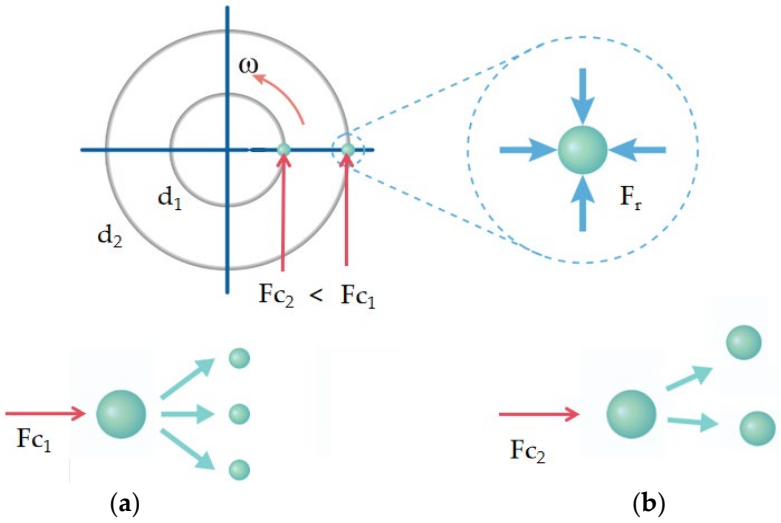


Figure 6. Schematic diagram of the influence of different cage diameters on droplet size. (**a**) shows a larger centrifugal force (Fc_1 corresponds to small droplet size and a large number of droplets); (**b**) shows a smaller centrifugal force (Fc_2 corresponds to larger droplet size and fewer droplets).

In addition, as the cage diameter increases, the rotational speed decreases (Figure 4), reducing the centrifugal force and consequently increasing the droplet diameter. However, in actual tests, the droplet diameter shows a decreasing trend. This indicates that although an increase in the cage diameter leads to a decrease in rotational speed, overall, the expansion of the cage diameter ultimately results in a smaller droplet diameter.

Under the same cage diameter and wind speed, as the flow rate increases, the droplet size generally shows an increasing trend. The main reason for this pattern is that an increase in the flow rate causes the liquid to accumulate inside the rotary cage, resulting in insufficient atomization and ultimately an increase in the droplet size. A schematic diagram of the influence of flow rate accumulation on droplet size is shown in Figure 7. In Figure 7a, under the same cage diameter and wind speed conditions, when the flow rate is high, more liquid accumulates inside the rotary cage, leading to insufficient atomization and an increase in the droplet size. When the flow rate is low, as shown in Figure 7b, the liquid passes directly through the mesh holes to form droplets, the liquid is fully atomized, and the droplet size is small. In addition, an increase in the flow rate also causes the liquid to accumulate in the rotary cage, which in turn increases the load on the rotary cage, leading to a decrease in rotational speed and an increase in droplet size.

Under the condition of the same flow rate and cage diameter, as the wind speed increases, the droplet size gradually decreases (Table 5). There are two main reasons for this. Firstly, an increase in wind speed will increase the rotational speed of the atomizer, resulting in a decrease in droplet size. Secondly, as the wind speed increases, the air shear force promotes the secondary atomization of the droplets ejected outside the cage, further reducing the droplet size.

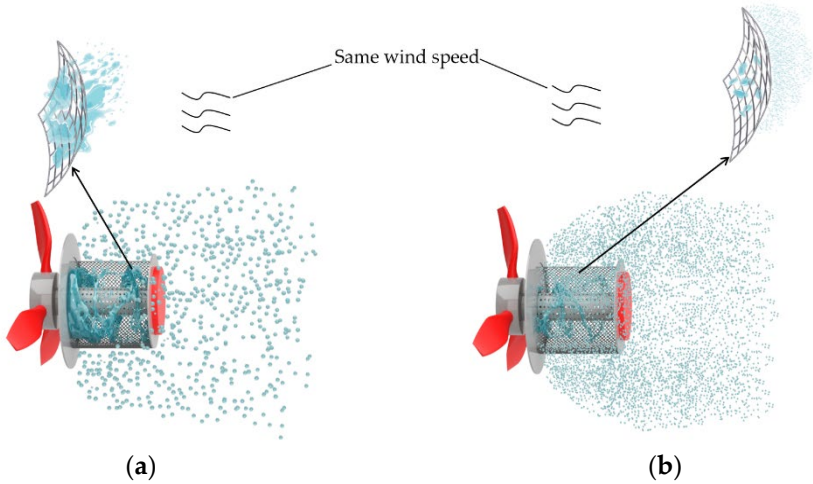


Figure 7. Schematic diagram of the effect of different flow rates on atomizer spray at the same wind speed and cage diameter. (**a**) High flow rate; (**b**) low flow rate.

3.2.2. Establishment of the Droplet Size Model

Correlation analyses evaluated the effects of wind speed, cage diameter, flow rate, and rotational speed on droplet size (Table 6). Wind speed had a highly significant negative correlation with droplet size ($r = -0.970$, $p = 0.001$). Rotation speed also showed a significant negative correlation with droplet size ($r = -0.924$, $p = 0.001$). Cage diameter exhibited a significant negative correlation as well ($r = -0.130$, $p = 0.019$). In contrast, the flow rate had no significant effect on droplet size, as its significance value was 0.439, greater than 0.05. However, compared with the impacts of wind speed and cage diameter, the influence of flow rate on droplet size is minimal. In comparison with the research findings under the condition of flow rates ranging from 0.66 to 1.33 L·min^{-1}, this result also demonstrates that, relative to wind speed, the influence of the flow rate of the rotary cage atomizer is not significant, which is consistent with the conclusion of this paper [34]. Comprehensive analysis reveals that among the parameters, wind speed has the greatest impact on droplet size, while flow rate has the least impact.

Table 6. Correlation analysis of droplet size with different wind speeds, flow rates, rotational speeds, and cage diameters.

Parameter	Wind Speed (m·s^{-1})	Flow Rate (L·min^{-1})	Cage Diameter (mm)	Rotational Speed (r·min^{-1})
Significance value	0.001	0.439	0.019	0.001
Correlation coefficient	−0.970	0.078	−0.130	−0.924

A linear regression model was used to establish the relationship between droplet size and rotational speed, cage diameter, flow rate, and wind speed. The goodness-of-fit R^2 of the model was 0.964, indicating that the changes in wind speed, cage diameter, and flow rate jointly explain 96.4% of the change in rotational speed. After collinearity diagnosis, the VIF values corresponding to wind speed, rotational speed, cage diameter, and flow rate were 11.3, 10.9, 5.5, and 1.8, respectively. The VIF values corresponding to cage diameter and flow rate were less than 10, which was within the acceptable range, but the VIF values of wind speed and rotational speed were greater than 10, representing that there was a multicollinearity problem in the linear regression model. To solve the multicollinearity problem, this study adopted the ridge regression model. By comparing the mean squared error (MSE) under different k values, finally, the k value with the minimum mean MSE ($k = 0.01$) was selected.

The results of the ridge regression analysis (Table 7) indicate that the overall fitting effect of the model is good. The adjusted R^2 is 0.947, suggesting that the model can explain 94.7% of the variation. By comparing the Bootstrap method with the ridge regression, it was found that the Bootstrap results were consistent with those of the ridge regression, indicating that the ridge regression model has a certain degree of robustness. The F-statistic coefficient is 661.172 ($p < 0.001$), indicating that the model as a whole has significant statistical significance. When other variables remain unchanged, for every 1 m/s increase in wind speed, the average droplet size decreases by 3.175 μm; for every 1 mm increase in cage diameter, the average droplet size decreases by 0.944 μm; and for every 1 r·min^{-1} increase in rotational speed, the average droplet size decreases by 0.032 μm.

Table 7. Results of ridge regression.

Variable	Coefficient	Significance Value
Wind speed	−3.175	0.008
Cage diameter	−0.944	0.000
Flow rate	0.859	0.185
Rotational speed	−0.032	0.015
Constant term	516.677	0.000
F-statistic	661.172	0.000
Adjusted R^2	0.947	

Similarly, the comparison between the predicted values and the measured values and the 10-fold cross-validation method were both adopted to evaluate whether the model was overfitted. The ridge regression model was verified by the measured data from 50 sets of rotating cage spray experiments. A comparative analysis was conducted on the predicted values and the actual values of the droplet size. The slope was relatively small, the R^2 of the fitted curve was 0.917, and there were no outliers, showing a good agreement. The results are shown in Figure 8. This indicates that the ridge regression model for the droplet size of the rotating cage atomizer is feasible. The evaluation was carried out using the 10-fold cross-validation method, and the results showed that the average mean squared error (MSE) of the droplet size prediction model was 133.7. This indicates that the prediction error of the model for unknown data is approximately 11.56 μm (the square root of the MSE). Both methods indicate that the droplet size prediction model has good generalization ability and there is no serious overfitting phenomenon.

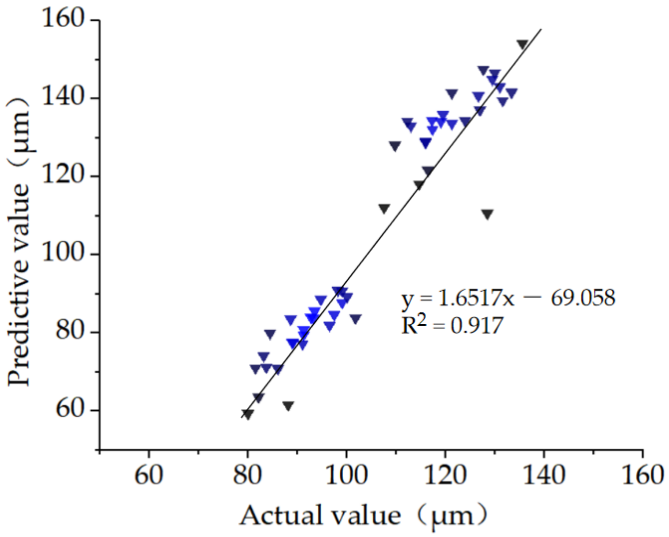


Figure 8. The predicted values and the actual values of the droplet size ridge regression model.

3.3. Analysis of the Influence of Flow Rate, Wind Speed, and Cage Diameter on RS

The smaller the droplet RS, the more uniform the atomization and the better the atomization effect. Figure 9 depicts the influence of the change in cage diameter on the droplet span distribution under the conditions of four different wind speeds and five different flow rates. Among them, five different colors represent five different flow rates. It can be seen from Figure 9 that, regardless of the cage diameter, the range of RS is within the interval of 1.55~2.0. To verify whether the influence of cage diameter on RS under different wind speed conditions is statistically significant, ANOVA was conducted on the relationship between the cage diameter and RS within different wind speed groups.

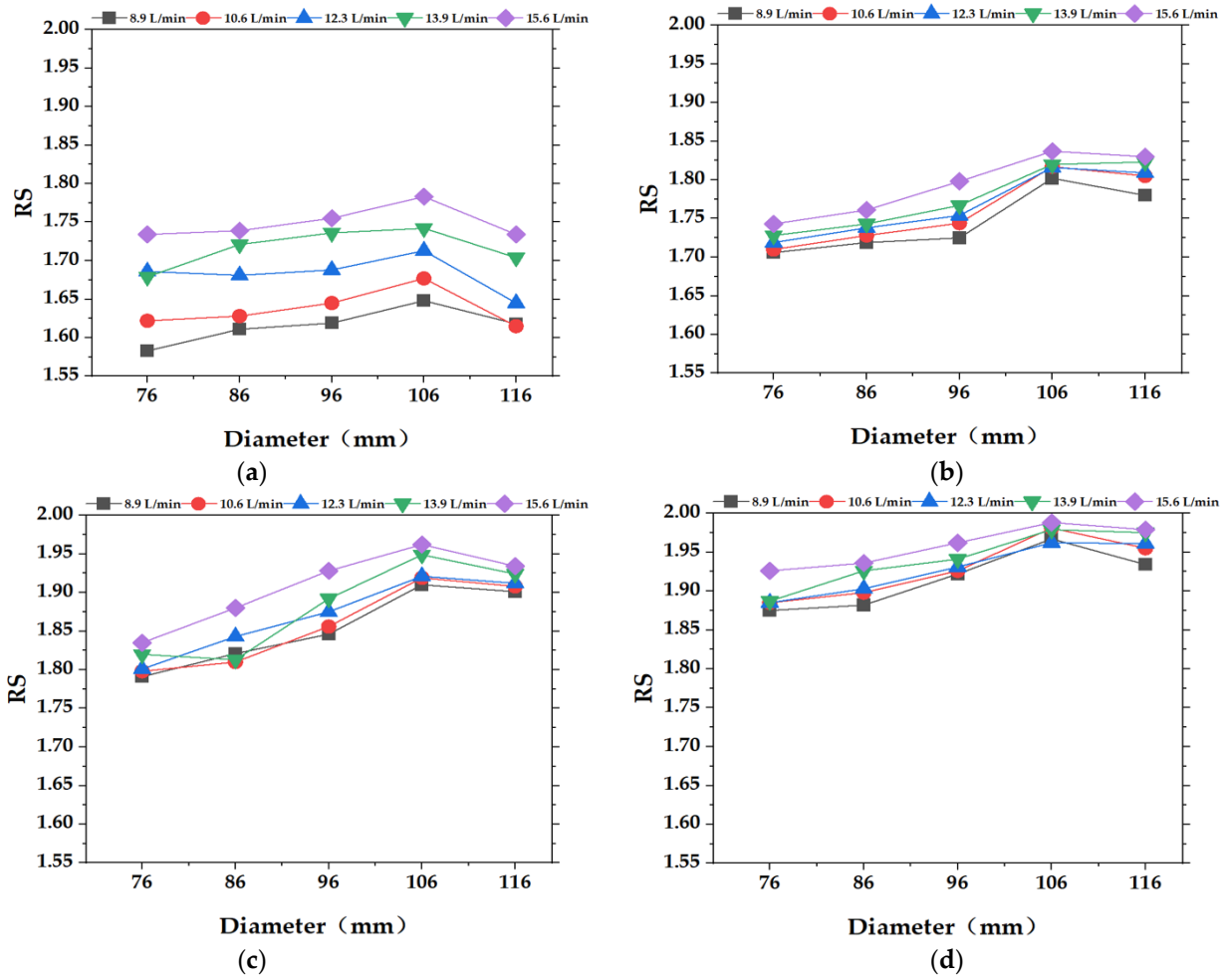


Figure 9. Relationship between cage diameter and RS under different flow rates and wind speeds. (**a**) Wind speed of 41.6 m/s; (**b**) 50 m/s; (**c**) 58.3 m/s; (**d**) 66.6 m/s.

The results of the ANOVA indicate that the degree to which the cage diameter affects RS varies under different wind speed conditions. When the wind speed is 41.6 m/s, the influence of different cage diameters on RS is not significant (p = 0.587, which is greater than 0.05). This suggests that under low wind speed conditions, changes in the cage diameter have a relatively small impact on RS. However, when the wind speeds are 50 m/s, 58.3 m/s and 66.6 m/s, the results of the one-way analysis of variance all show that the influence of different cage diameters on RS is significant (p = 0.0001, which is less than 0.05).

As can be seen from Figure 9, as the cage diameter increases, the value of RS first increases and then decreases. The rotating cage with a cage diameter of 106 mm usually has the highest RS value. This may indicate that there is an upper limit for RS. Once this upper limit is exceeded, the RS will no longer increase with the increase in cage diameter. It is

speculated that the reason is as follows: during the stage when RS is rising, the increase in the cage diameter will lead to an increase in the surface area of the rotating cage, allowing more liquid to adhere to the surface, which makes it impossible for some of the liquid to be fully atomized. During the stage when RS is decreasing, the continuous increase in cage diameter leads to an increase in centrifugal force, and more large droplets will be atomized into smaller droplets, resulting in a relatively uniform distribution of the droplets. When compared with the study on the RS of the rotary disk atomizer, the results show that there is a correlation between RS in the rotary disk atomizer and the ratio of the measurement distance of the droplets downstream to the diameter of the rotary disk. That is, as the diameter of the rotary disk increases, the uniformity of the droplets increases [35], which is partially consistent with the conclusion of this paper. The difference lies in the fact that the inflection point of RS appears in this paper, while no inflection point of RS has been found in the rotary atomize. This may be due to the difference in the types of atomizers.

Comparing Figure 9a–d, which show the influence of wind speed on RS, we can see that at a wind speed of 41.6 m/s, the RSs corresponding to different flow rates are relatively scattered. Under the other three wind speeds, the RSs corresponding to different flow rates are relatively concentrated. Moreover, under the same cage diameter and the same flow rate, as the wind speed increases, RS shows an upward trend. The reasons considered are as follows: At lower wind speeds, the air shear force on the droplets is relatively small, so the droplets remain relatively intact and are more evenly distributed. However, at higher wind speeds, the air shear force on the droplets increases significantly and some small droplets combine to form larger ones, thus affecting the RS. Compared with the results of this research on pressure nozzles, this research indicates that as the wind speed increases, the RS increases. Ref. [36], which is consistent with the conclusion of this study. In addition, high wind speeds can accelerate the evaporation of droplets [37], especially small-size droplets, which are more likely to evaporate rapidly, thus further increasing the RS.

As the flow rate increases, the RS shows a gradually increasing trend. Under the same wind speed and cage diameter, the RS is the largest when the flow rate is 15.6 L·min^{-1}. The possible reasons considered are as follows: As the flow rate increases, more liquid accumulates inside the rotating cage. The atomization capacity of the atomizer is limited. Part of the liquid is atomized into small droplets as normal, while another part is ejected before it can be atomized. This causes an uneven distribution of droplets, leading to an increase in the RS. In comparison with the conclusion of the research on pressure nozzles, the results of this study indicate that with the increase in flow rate, RS does not show a uniform changing trend [38]. A possible reason is that the structure of the pressure nozzle restricts its atomization uniformity and makes it difficult to control.

4. Conclusions

(1) When other variables remain constant, for every 1 m/s increase in wind speed, the average droplet size decreases by 3.175 μm. For every 1 mm increase in the cage diameter, the average droplet size decreases by 0.944 μm, and the droplet size is the smallest when the cage diameter is 76 mm. The droplet size model for the droplets atomized by the atomizer yielded an R^2 of 0.917 between its predicted and measured values.

(2) The rotation speed increases as the wind speed increases; the cage diameter is negatively correlated with the rotation speed. When other variables remain constant, for every 1 r·min^{-1} increase in rotational speed, the average droplet size decreases by 0.032 μm.

(3) Statistical analysis indicates that the effect of cage diameter on RS is significantly affected by wind speed. Under the condition of wind speed of 41.6 m/s, the cage

diameter has no significant impact on RS. However, under wind speed conditions of 50 m/s, 58.3 m/s, and 66.6 m/s, the cage diameter has a significant effect on RS. Moreover, as the cage diameter increases, RS shows a trend of first increasing and then decreasing. Among them, the RS of the 106 mm rotating cage is usually the highest. As the wind speed rises, RS gradually increases; as the flow rate increases, RS also increases.

This study contributes to the development of an atomizer prototype and provides a theoretical reference for the operation parameters of large-load plant protection UAVs, such as the selection of cage diameter. Besides the influence of cage diameter, droplet size is also affected by factors such as additives and the mesh number of the rotating cage. Currently, only a few discrete values such as 76 mm, 86 mm, 96 mm, 106 mm, and 116 mm have been tested, and the gradient of cage diameter settings is limited. To have a more comprehensive understanding of the relationship between cage and droplet size, in the next step of this study, two main actions will be taken. Firstly, experiments will be carried out using rotating cages with different mesh numbers and adding additives. Secondly, the gradient of the cage diameter will be increased. In addition, field experiments will be carried out on large-load plant protection UAVs equipped with the atomizer.

Author Contributions: Conceptualization, R.Z. and J.Y.; methodology, J.Y.; software, J.Y.; validation, L.L., Q.T., and J.Y.; formal analysis, J.Y.; investigation, J.Y. and R.Z.; resources, R.Z.; data curation, J.Y., W.Y., and P.H.; writing—original draft preparation, J.Y.; writing—review and editing, J.Y., L.L., and R.Z.; visualization, J.Y.; supervision, R.Z.; project administration, R.Z.; funding acquisition, R.Z. All authors have read and agreed to the published version of the manuscript.

Funding: This work was supported by the National Key R&D Program of China (2023YFD2000204) National Natural Science Foundation of China (32472008), and the Major Scientific and Technological Achievements Cultivation Project of the BAAFS.

Data Availability Statement: The original contributions presented in the study are included in the article; further inquiries can be directed to the corresponding author.

Conflicts of Interest: The authors declare no conflicts of interest.

References

1. Nahiyoon, S.A.; Ren, Z.; Wei, P.; Li, X.; Li, X.; Xu, J.; Yan, X.; Yuan, H. Recent Development Trends in Plant Protection UAVs: A Journey from Conventional Practices to Cutting-Edge Technologies—A Comprehensive Review. *Drones* **2024**, *8*, 457. [CrossRef]
2. Deng, Q.; Zhang, Y.; Lin, Z.; Gao, X.; Weng, Z. The Impact of Digital Technology Application on Agricultural Low-Carbon Transformation—A Case Study of the Pesticide Reduction Effect of Plant Protection Unmanned Aerial Vehicles (UAVs). *Sustainability* **2024**, *16*, 10920. [CrossRef]
3. Ganesh, K.; Siva, S.; Abhishek, G.A. comprehensive review on payloads of unmanned aerial vehicle. *Egypt. J. Remote Sens. Space Sci.* **2024**, *27*, 637–644. [CrossRef]
4. Yang, S.; Yang, X.; Mo, J. The application of unmanned aircraft systems to plant protection in China. *Precis. Agric.* **2018**, *19*, 278–292. [CrossRef]
5. Wang, G.; Han, Y.; Li, X.; Andaloro, J.; Chen, P.; Hoffmann, C.; Han, X.; Chen, S.; Lan, Y. Field evaluation of spray drift and environmental impact using an agricultural unmanned aerial vehicle (UAV) sprayer. *Sci. Total Environ.* **2020**, *737*, 139793. [CrossRef]
6. Calderone, G.; Ferro, M.V.; Catania, P. A systematic literature review on recent unmanned aerial spraying systems applications in orchards. *Smart Agric. Technol.* **2025**, *10*, 100708. [CrossRef]
7. Hong, S.W.; Park, J.; Jeong, H.; Lee, S.; Choi, L.; Zhao, L.; Zhu, H. Fluid Dynamic Approaches for Prediction of Spray Drift from Ground Pesticide Applications: A Review. *Agronomy* **2021**, *11*, 1182. [CrossRef]
8. Ashenafi, T.D.; Mulugeta, A.D.; Kris, R.; Donald, D.; David, N.; Dany, B.; Bart, M.; Nicolai, P.V. Development and validation of a 3D CFD model of drift and its application to air-assisted orchard sprayers. *Biosyst. Eng.* **2017**, *154*, 62–75.
9. Richard, B.; Greg, G.; Farah, A.; Brian, L.; Carol, R.; Brian, F.; Abby, L.; Greg, K.; Dan, P. Winds of change, developing a non-target plant bioassay employing field-based pesticide drift exposure: A case study with atrazine. *Sci. Total Environ.* **2019**, *678*, 239–252.

10. Martin, D.E.; Perine, J.W.; Grant, S.; Abi-Akar, F.; Henry, J.L.; Latheef, M.A. Spray Deposition and Drift as Influenced by Wind Speed and Spray Nozzles from a Remotely Piloted Aerial Application System. *Drones* **2025**, *9*, 66. [CrossRef]
11. Li, G.; Chen, L.; Li, L.; Yi, T.; Ding, C.; Wang, J.; Zhao, C.; Zhang, R. Modeling and Experimental Validation of the Atomization Efficiency of a Rotary Atomizer for Aerial Spraying. *Agronomy* **2022**, *12*, 419. [CrossRef]
12. Craig, I.P.; Hewitt, A.; Terry, H. Rotary atomiser design requirements for optimum pesticide application efficiency. *Crop Prot.* **2014**, *66*, 34–39. [CrossRef]
13. Elsaied, S.; Tarek, F.; Mohamed, D.; Nada, E.; Mayie, A. An electrical rotary cage atomizer fabricated for spraying orchard. Management. *Econ. Eng. Agric. Rural. Dev.* **2021**, *21*, 495–502.
14. Teske, M.E.; Thistle, H.W.; Hewitt, A.J.; Kirk, I.W.; Dexter, R.W.; Ghent, J.H. Rotary atomizer drop size distribution database. *Trans. AEAE* **2005**, *48*, 917–921.
15. Hewitt, A.J. Droplet size spectra classification categories in aerial application scenarios. *Crop Prot.* **2008**, *48*, 1284–1288. [CrossRef]
16. Matsushita, Y.; Tomoyuki, K.; Yasuhiro, S.; Yoshiya, M.; Takahiro, O.; Minori, S.; Takao, I.; Masatoshi, D.; Junichi, F.; Hideyuki, A. A spray painting simulation using high-speed rotary Atomizer—Model development and comparison of LES and RANS. *Results Eng.* **2024**, *21*, 101–697. [CrossRef]
17. Maximilian, K.; Tórstein, V.; Joensen, M.; Roisman, C. Study of the internal flow in a rotary atomizer and its influence on the properties of the resulting spray. *Int. J. Multiph. Flow* **2018**, *100*, 30–40.
18. Tang, Q.; Chen, L.; Zhang, R.; Xu, M.; Xu, G.; Zhang, b. Design and test of IEA-I high speed wind tunnel for aerial plant protection. *Trans. CSAE* **2016**, *32*, 73–81.
19. Malvern Instruments Ltd. *Spraytec User Manual*; MAN0368 Issue 2.0; Malvern Instruments Ltd.: Malvern, UK, 2006; pp. 10(2)–10(4).
20. Hooper, G.H.S.; Peter, S. Droplet size spectra produced by the atomization of a ULV formulation of fenitrothion with a Micronair AU5000 rotary atomizer. *Crop Prot.* **1995**, *14*, 27–30. [CrossRef]
21. Micronair, Ltd. *Micronair AU5000 Atomizer Operation Manual and Parts Catalog Manual*; Micronair, Ltd.: Herefordshire, UK, 1990; pp. 20–23.
22. Zhao, C.; Chai, S.; Chen, L.; Zhang, R.; Li, L.; Tang, Q. Establishment and Experiment of Quadratic Residual Compensation Atomization Model of Electricity Atomizer. *Trans. CSAE* **2020**, *51*, 19–27, 37.
23. Azevedo, G.O.d.A.; Fernandes, B.J.T.; Silva, L.H.d.S.; Freire, A.; de Araújo, R.P.; Cruz, F. Event-Based Angular Speed Measurement and Movement Monitoring. *Sensors* **2022**, *22*, 7963. [CrossRef]
24. Xing, W.; Cui, Y.; Wang, X.; Shen, J. Optimization of Operational Parameters of Plant Protection UAVs. *Sensors* **2024**, *24*, 5132. [CrossRef]
25. Du, S. The operation method of ultra-low-volume spraying with airplane. *J. Northeast. For. Univ.* **1996**, *7*, 45–50.
26. Ranabhat, S.; Price, R. Effects of Flight Heights and Nozzle Types on Spray Characteristics of Unmanned Aerial Vehicle (UAV) Sprayer in Common Field Crops. *AgriEngineering* **2025**, *7*, 22. [CrossRef]
27. Kumar, A.; Singh, S.; Yadav, M.; Bhuj, B.; Dhar, S.; Pruthi, N.; Kumar, R.; Bajpai, V.; Rizwan, M.; Jyoti, K.; et al. Artificial Intelligence, Internet of Things (lot) and Smart Agriculture for Sustainable Farming: A Review. *Ann. Plant Sci.* **2022**, *11*, 5512–5564.
28. Hewitt, A.J.; Johnson, D.R.; Fish, J.D.; Hermansky, C.G.; Valcore, D.L. Development of the Spray Drift Task force database for aerial applications. *Environ. Toxicol. Chem.* **2002**, *21*, 648–658. [CrossRef]
29. Basílio, S.; Furtado Júnior, M.R.; de Alvarenga, C.B.; Vitória, E.L.d.; Vargas, B.C.; Privitera, S.; Caruso, L.; Cerruto, E.; Manetto, G. Effect of Adjuvants on Physical–Chemical Properties, Droplet Size, and Drift Reduction Potential. *Agriculture* **2024**, *14*, 2271. [CrossRef]
30. He, Y.; Wu, J.; Fu, H.; Sun, Z.; Fang, H.; Wang, W. Quantitative Analysis of Droplet Size Distribution in Plant Protection Spray Based on Machine Learning Method. *Water* **2022**, *14*, 175. [CrossRef]
31. Nuyttens, D.; Baetens, K.; De Schampheleire, M.; Sonck, B. Effect of nozzle type and pressure on spray droplet characteristics. *Biosyst. Eng.* **2021**, *97*, 333–345. [CrossRef]
32. Elizabeth, M.; Qi, L.; Wu, Y. Evaluation of droplets size distribution and velocity pattern using Computational Fluid Dynamics modelling. *Comput. Electron. Agric.* **2019**, *164*, 104886.
33. Ru, Y.; Zhu, C.; Bao, R.; Li, Z.; Ding, T. Droplet size distribution of aerial nozzle for plant protection in wind tunnel and flight conditions. *Trans. CSAE* **2016**, *32*, 94–98.
34. Zhang, H.; Zheng, J.; Zhou, H.; Song, W.; Ge, Y. Performance experiments of rotary cage atomizer for biological pesticide application. *Trans. CSAE* **2013**, *29*, 63–70.
35. Ahmed, M.; Youssef, M.S. Characteristics of Mean Droplet Size Produced by Spinning Disk Atomizers. *J. Fluids Eng.—Trans. ASME* **2012**, *134*, 071103. [CrossRef]
36. Hoffmann, W.C.; Fritz, B.K.; Lan, Y. Evaluation of a Proposed Drift Reduction Technology High-Speed Wind Tunnel Testing Protocol. *J. ASTM Int.* **2009**, *6*, 11. [CrossRef]

37. Deng, W.; Ding, W.; He, X. Droplet velocity and energy characteristics of continuously variable spray based on pulse width modulation. *Trans. CSAE* **2009**, *25*, 66–69.
38. Fan, S.; Chen, S.; Wu, Z.; Wu, S.; Chen, Y.; Liu, D.; Yao, Y.; Huang, J. Analysis of droplet size distribution and selection of spray parameters based on the fractal theory. *J. Clean. Prod.* **2022**, *371*, 133315. [CrossRef]

Disclaimer/Publisher's Note: The statements, opinions and data contained in all publications are solely those of the individual author(s) and contributor(s) and not of MDPI and/or the editor(s). MDPI and/or the editor(s) disclaim responsibility for any injury to people or property resulting from any ideas, methods, instructions or products referred to in the content.